Photo-double-ionization of water at 20 eV above threshold

J. M. Randazzo [1,*], G. Turri,[2] P. Bolognesi [3], J. Mathis,[2] L. U. Ancarani,[4] and L. Avaldi [3]

[1]*Instituto Balseiro and CONICET, CP 8400 San Carlos de Bariloche, Rio Negro, Argentina*
[2]*Embry-Riddle Aeronautical University, Physical Sciences Department, 600 South Clyde Morris blvd, Daytona Beach, Florida 32114, USA*
[3]*CNR-Istituto di Struttura della Materia, Area della Ricerca di Roma 1, CP10, 00015 Monterotondo Scalo, Italy*
[4]*Université de Lorraine, CNRS, LPCT, F-57000 Metz, France*

The photodouble ionization of the water molecule is studied at 20 eV excess energy in a combined experimental and theoretical investigation. In the experiments, two photoelectrons of equal kinetic energy are detected in coincidence after energy and angular selection. On the theoretical side, a generalized Sturmian function approach is implemented to describe accurately the correlated two-electron continuum, while separable products of Moccia orbitals [J. Chem. Phys. **40**, 2164 (1964)] are used for the initial electronic state of the water molecule. The theoretical triple-differential cross sections (TDCSs) are averaged over all possible molecular orientations in order to be compared with the experiments. The measured TDCSs display rich angular distributions that are in large part well reproduced by the adopted first-order treatment of the interaction with a two-active-electron target.

I. INTRODUCTION

The photodouble ionization (PDI) of atomic and molecular targets by single-photon absorption has received special attention in the last years because it provides a suitable tool to get a detailed understanding of quantum ionization mechanisms due to electron correlation. Indeed, during the process, one of the indistinguishable electrons interacts with the photon, acquiring energy and momentum, and it is through the electronic correlation that the double-ionization occurs [1,2].

For the helium atom, after PDI we are left with a pure Coulomb three-body scattering problem. The triple-differential cross sections (TDCSs) completely describe the dynamics of the two electrons together with the residual dication final state in the different asymptotic energy regimes. Experimentally, TDCS can be obtained through coincidence detection of the two correlated electrons, selected in angle of emission and kinetic energy [3]. The extension to the molecular H_2 case has been deeply investigated; complete experiments involving the detection of the two electrons and a proton allowed a reconstruction of the molecular geometry at the time of the photoionization [4,5]. Both experimental and theoretical studies lead to a detailed understanding of PDI in two-electron systems like the He atom and the H_2 molecule [1].

Measurements of the TDCS in the molecular frame cannot be done for more complex targets where dication states have barriers to dissociation, and the multicenter Coulomb potential effects have to be investigated with the TDCS averaged over all spatial orientations of the molecule. Moreover, while in an atom the threshold for the PDI is well defined, an entire threshold region exists in a molecule defined by the potential-energy surface of the neutral ground and final dication states. In this region two kind of processes compete: (i) the direct promotion of the two correlated electrons to the continuum, and (ii) the indirect process given by the formation of an excited cation state embedded in the double continuum, followed by a secondary electron emission.

These two mechanisms have been clearly observed in water by Truong *et al.* [6] and Eland [7] in near-threshold measurements of the binding-energy spectrum of the dication, and more recently [8,9] in the investigation of the two-body ($OH^+ + H^+ + 2e^-$) and three-body ($2H^+ + O + 2e^-$) ionic fragmentation channels combining electron-ion imaging techniques [8] with a classical trajectory method [9]. No angular-resolved measurements involving the coincidence detection of two electrons at several eV above threshold have been reported for water, apart from our preliminary report [10]. As far as angular-resolved measurements for other molecules are concerned, to the best of our knowledge, only N_2 data have been previously reported [11].

As the theoretical description of the PDI process is concerned, almost numerically exact and gauge-invariant results are available for the prototypal two-electron system (see, for example, Ref. [12] and references therein). Two active electron models have also been successfully applied to deal with PDI of many electron atoms (see, e.g., Ref. [13]). For the molecular case, single-centered approaches have been used for H_2 [14], while the first nonperturbative approach was presented by Vanroose and collaborators [15]. Modeling the PDI in more complex (diatomic or tri-atomic) molecules is an extremely challenging task, due to the number of degrees of freedom, the many competing PDI mechanisms, and the difficulty of describing the two free electrons in a Coulomb field generated by several centers.

In the present investigation we have measured the relative TDCS of water at two photon energies $\hbar\omega$ (63 and 65 eV) by detecting two photoelectrons of equal energy (10 eV). The

*Corresponding author: randazzo@cab.cnea.gov.ar

direction of one electron has been fixed at $0°$, $30°$, or $60°$ with respect to the polarization axis of the incident radiation, while the other one has been detected over the $110° - 290°$ range of emission angles. At similar photon energies, Reedy *et al.* [8] observed that the PDI of H_2O leads mainly to the $OH^+ +$ H two-body dissociation with a minor contribution of the $2H^+ + O^*$ three-body one. In our experiment the ions are not detected, thus the measured TDCS cannot be associated with a particular dissociation channel. We have also calculated the TDCS for the direct PDI of the molecule considering products of the well-known Moccia orbitals [16] as initial states, and a generalized Sturmian function (GSF) approach to describe the two-electron continuum. In our calculation, the geometry of the molecule and its orientation is included through the initial-state description. Once the TDCS are evaluated, they are averaged over all possible molecular orientations in order to be compared with the measured data.

The remainder of this paper is organized as follows: Section II is devoted to some experimental details of the setup, while the theoretical model is described in Sec. III. The experimental results are collected and compared with our theoretical calculations in Sec. IV. Finally, in Sec. V some concluding remarks are presented.

II. EXPERIMENT

The experiments have been performed at the gas phase photoemission beam-line of the Elettra storage ring using the multicoincidence end-station [1]. The incident radiation is provided by an undulator source and is 100% linearly polarized. Two independently rotatable turntables are housed in the vacuum chamber. Seven hemispherical electrostatic spectrometers are mounted at $30°$ angular intervals on a turntable that rotates in the plane perpendicular to the direction z of propagation of the incident radiation. Three other spectrometers are mounted at $\theta_1 = 0°$, $30°$, and $60°$ with respect to the polarization vector of the light on a smaller turntable. In these measurements both arrays have been kept in the perpendicular plane, and the seven analyzers in the larger frame as well as the one in the smaller frame have been set for the detection of electrons of the same kinetic energy, $E_1 = E_2 \simeq 10$ eV. The energy resolution and the angular acceptance in the dispersion plane of the spectrometers were ΔE_1, $\Delta E_2 \simeq 0.3$ eV and $\Delta \theta_1$, $\Delta \theta_2 = \pm 4°$. The angular distribution is obtained by successive rotations of the larger frame, which allowed us to cover a range of emission angles between $113°$ and $290°$. The relative efficiency of the ten spectrometers has been calibrated by measuring known photoelectron angular distributions at 10 eV above their respective ionization thresholds. The same efficiency correction has been assumed for the coincidence measurements. The procedure used to determine the relative efficiency of the analyzers has been described in detail in Ref. [17] and will not be repeated here. Typical coincidence count rates were in the range of a few mHz. All the coincidence yields reported in the figures shown in Sec. IV are on the same relative scale of counts.

III. THEORY

The double-ionization process is described by a stationary scattering wave function obtained from a perturbative series

where the zeroth order corresponds to the initial state, the first order to the single-photon absorption case, and so on. We take here the same first-order approach adopted for helium PDI calculations [12]. Considering the number of active electrons of the H_2O molecule and its complex (nonspherical) structure, we have made some approximations. The first one is to consider the independent-particle model for the initial water ground state, corresponding to the orbitals $1A_1$, $2A_1$, $3A_1$, $1B_2$, and $1B_1$. Then we consider one or two of them to be affected by the absorption of the photon while the rest of the orbitals remain unperturbed, defining a charge-density distribution which, together with the atomic cores, determines the molecular dication potential for the two electrons ejected into the continuum. A further approximation corresponds to taking the spherical average of this potential: this allows us to have spherical symmetry of the scattering Hamiltonian and thus to express the solution in terms of total angular-momentum eigenfunctions. As a consequence, the average of the cross section over the initial orientation of the molecule can be performed exactly.

Within this set of approximations, the scattering wave function describing the two electrons in the continuum is obtained numerically, from the corresponding driven equations, through a GSF approach as in the study of PDI of helium [12]. We should mention here that our numerical GSF results reproduced very accurately, and on an absolute scale, benchmark calculations themselves in excellent agreement with experimental data.

A. Initial state

Following recent investigations on photoionization [18] and bare ion impact ionization of molecular targets [19,20], we consider an independent-particle model for the molecular initial electronic state; each two-electron state can be considered as a (spin-symmetrized) product of single-centered normalized molecular orbitals,

$$\phi_j(\mathbf{r}) = \sum_{i=1}^{N_j} B_{l_i,m_i,n_i}^{(j)} \mathcal{R}_{n_i}^{(j)}(r) Y_{l_i}^{m_i}(\hat{\mathbf{r}}) = \sum_{i=1}^{N_j} R_{l_i,m_i}^{(j)}(r) Y_{l_i}^{m_i}(\hat{\mathbf{r}}), \quad (1)$$

where

$$\mathcal{R}_{n_j}(r) = \left[\frac{(2\zeta_j)^{2n_j+1}}{(2n_j)!} \right]^{1/2} r^{n_j-1} e^{-\zeta_j r} \quad (2)$$

are Slater orbitals, and $B_{l_i,m_i,n_i}^{(j)}$ and ζ_i are tabulated coefficients [16].

Each ϕ_j orbital is described in spherical coordinates with respect to the oxygen atom, where the molecular orientation, i.e., the positions of the hydrogen atoms, are fixed in space. Rotations of the molecule, in terms of three Euler angles (α, β, γ), modify only the angular variables as accounted for by the well-known relation

$$Y_{lm}(\theta, \varphi) = \sum_{m'=-l}^{l} D_{m',m}^{l}(\alpha, \beta, \gamma) Y_{lm'}(\theta', \varphi'), \quad (3)$$

where θ and φ are the angles in the rotated reference frame while θ' and φ' are the variables in the original frame; $D_{m',m}^{l}$ are the Wigner D-matrix elements [21,22].

TABLE I. Partial-wave weights of the radial terms for the initial two electron states $(3a_1)^{-1}(1b_2)^{-1}\,^1A_2$ and $(3a_1)^{-2}\,^1A_1$. The cumulative sum (c.s.) is used to determine convergence.

| L_0 | M_0 | $(3a_1)^{-1}(1b_2)^{-1}\,^1A_2$ | | L_0 | M_0 | $(3a_1)^{-2}\,^1A_1$ | | # |
		Weight	c. s.			Weight	c. s.	
1	−1	0.2520	0.2520	0	0	0.2932	0.2932	1
1	1	0.2520	0.5040	1	0	9.9074×10^{-2}	0.3923	2
2	−1	0.2270	0.7310	2	−2	5.144×10^{-3}	0.3975	3
2	1	0.2270	0.9580	2	0	0.5819	0.9794	4
3	−3	3.3070×10^{-3}	0.9613	2	2	5.1438×10^{-3}	0.9845	5
3	−1	1.5587×10^{-2}	0.9769	3	−2	3.5127×10^{-3}	0.9880	6
3	1	1.5587×10^{-2}	0.9924	3	0	4.4722×10^{-3}	0.9925	7
3	3	3.3070×10^{-3}	0.9958	3	2	3.5127×10^{-3}	0.9960	8

Let us approximate the initial two-electron (labeled 1 and 2) wave function as a single product of two orbitals ϕ_j. In terms of the total angular-momentum eigenfunctions it reads

$$\Psi_0(\mathbf{r}_1, \mathbf{r}_2) = \phi_1(\mathbf{r}_1)\phi_2(\mathbf{r}_2) = \sum_{L_0=L_{0,\min}}^{L_{0,\max}} \sum_{M=-L_0}^{L_0} \psi_0^{L_0,M_0}(\mathbf{r}_1, \mathbf{r}_2),$$

(4)

with

$$\psi_0^{L_0,M_0}(\mathbf{r}_1, \mathbf{r}_2) = \sum_{l_1,l_2} R_{l_1,l_2}^{L_0,M_0}(r_1, r_2)\mathcal{Y}_{l_1,l_2}^{L_0,M_0}(\hat{\mathbf{r}}_1, \hat{\mathbf{r}}_2),$$

(5)

where

$$R_{l_1,l_2}^{L_0,M_0}(r_1, r_2) = \sum_{m_1} R_{l_1,m_1}^{(1)}(r_1) \sum_{m_2} R_{l_2,m_2}^{(2)}(r_2)\langle l_1, l_2; m_1, m_2 | L_0, M_0\rangle.$$

(6)

$\mathcal{Y}_{l_1,l_2}^{L_0,M_0}$ are the bispherical harmonics and $\langle l_1, l_2; m_1, m_2 | L_0, M_0\rangle$ are the Clebsch-Gordan coefficients [21,22].

By using standard properties of the rotation D-matrix, it is easy to show that the bispherical harmonics transform according to

$$\mathcal{Y}_{l_1,l_2}^{L_0,M_0}(\hat{\mathbf{r}}_1, \hat{\mathbf{r}}_2) = D_{M_0,M_0}^{L_0}(\gamma, \beta, \alpha)\mathcal{Y}_{l_1,l_2}^{L_0,M_0}(\hat{\mathbf{r}}_1', \hat{\mathbf{r}}_2'),$$

(7)

a relation that connects each partial wave from the unrotated system to the rotated one.

To have an idea of how many L_0 terms one should consider, we have looked at their individual importance for each possible initial two-electron state. Integration of the square modulus of each partial wave over the coordinates $\mathbf{r}_1$ and $\mathbf{r}_2$:

$$\int d^3\mathbf{r}_1 \int d^3\mathbf{r}_2 \big|\psi_0^{L_0,M_0}(\mathbf{r}_1, \mathbf{r}_2)\big|^2,$$

(8)

provides a measure of their weights. In Table I we show the typical convergence pattern for two of the initial states considered in the application presented in Sec. III. Clearly, we see that eight (L_0, M_0) pairs provide a satisfying convergence in their description.

B. Molecular dication potential for the outgoing electrons

Once the two electrons are promoted to the single and double continua, the other target electrons, together with the three Coulomb centers, are used to define a dication molecular potential for each electron (here identified by the index $i = 1$ or 2). Disregarding the exchange term, we consider the static potential

$$V_{i,\text{mol}}(\mathbf{r}_i) = -\sum_{n=1}^{3} \frac{Z_n}{|\mathbf{r}_i - \mathbf{R}_n'|} + \sum_{j=1}^{N_{MO}} \mathcal{N}_{ij} \int d\mathbf{x} \frac{|\tilde{\phi}_j(\mathbf{x})|^2}{|\mathbf{r}_i - \mathbf{x}|},$$

(9)

where $\mathcal{N}_{ij} = 2 - \delta_{1j} - \delta_{2j}$, Z_n are the nuclear charges, and $\mathbf{R}_n'$ are their positions (the prime denotes that they are being referenced to the unrotated system); in the last term, the sum runs over the N_{MO} molecular orbitals (where the tilde denotes that they are being referenced to the unrotated system). Using the partial-wave series for the orbitals, the standard multipole expansion for the Coulomb interaction and property (3), the average over the all molecular orientation yields a spherically symmetric potential

$$\mathcal{U}_{i,\text{mol}}(r_i) = \frac{1}{8\pi^2} \int_0^{\pi} \sin\beta d\beta \int_0^{2\pi} d\alpha \int_0^{2\pi} d\gamma V_{i,\text{mol}}(\mathbf{r}_i)$$

(10a)

$$= -\sum_{n=1}^{3} \frac{Z_n}{R_>} + \sum_{j=1}^{N_{MO}} \mathcal{N}_{ij} F_j(r),$$

(10b)

where

$$F_j(r) = \sum_{l_i,m_i} \left[\frac{1}{r} \int_0^r r'^2 dr' \big|R_{l_i,m_i}^j(r')\big|^2 + \int_r^{\infty} r' dr' \big|R_{l_i,m_i}^j(r')\big|^2 \right].$$

(11)

Similar averages have been used to study single-ionization processes [18–20]. Figure 1 shows the averaged effective charge (the potential multiplied by the radial distance r) obtained by removing the two electrons from different pairs of orbitals. The potential experienced by the photoelectrons varies from that generated by the oxygen nuclear charge -8 to -2, corresponding to the asymptotic dication potential. The small dip, located at about $r = 1.814$ a.u., corresponds roughly to the equilibrium position of each H atom.

C. Two-electron scattering wave function and cross sections

Once the initial state and central potential are defined, the following velocity gauge driven equation can be written for
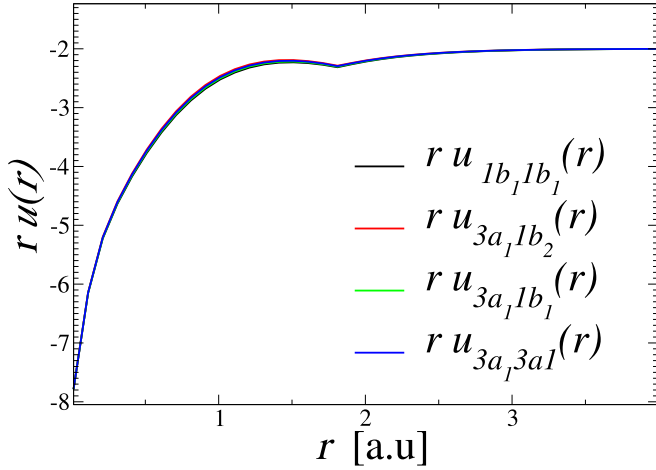
FIG. 1. Radial variation of the angular averaged effective charge [potential $r\,\mathcal{U}_{i,\mathrm{mol}}(r)$] obtained by removing electrons from four different pairs of molecular orbitals.

the two-electron continuum [12]:

$$
\left[\sum_{i=1}^{2} h_i + \frac{1}{r_{12}} - E\right]\Psi_{sc}(\mathbf{r}_1, \mathbf{r}_2) = \varepsilon \cdot \sum_{i=1}^{2}\nabla_i\Psi_0(\mathbf{r}_1, \mathbf{r}_2), \quad (12)
$$

where $h_i = -\frac{1}{2}\nabla_i^2 + \mathcal{U}_i(r_i)$. In the length gauge a similar equation can be written, with $\omega\varepsilon\cdot\sum_{i=1}^{2}\mathbf{r}_i\Psi_0(\mathbf{r}_1, \mathbf{r}_2)$ as the driven term. Considering the spherical symmetry of the Hamiltonian, we can propose a partial-wave expansion of the scattering wave function:

$$
\Psi_{sc}(\mathbf{r}_1, \mathbf{r}_2) = \sum_{L_0, M_0} D_{M_0, M_0}^{L_0}(\alpha, \beta, \gamma)\sum_{L, M}\psi_{sc}^{L, M}(\mathbf{r}_1', \mathbf{r}_2'), \quad (13)
$$

with each partial-wave term satisfying

$$
\left[\sum_{i=1}^{2} h_i + \frac{1}{r_{12}} - E\right]\psi_{sc}^{L, M}(\mathbf{r}_1, \mathbf{r}_2) = \varepsilon \cdot \sum_{i=1}^{2}\nabla_i\psi_0^{L_0, M_0}(\mathbf{r}_1, \mathbf{r}_2),
$$
$$(14)$$

and an equivalent equation for the length gauge.

We end up with a Hamiltonian averaged in molecular orientations (a spherical approach for the dication potential) which includes the correlation of the two electrons in the continuum exactly. Combining the many partial waves, we are also taking into account the molecular structure and its orientation which we can change through the Wigner matrix. We solve Eq. (14) numerically with the generalized Sturmian method as done for helium [12]. This time, gauge invariance is not expected since the initial state is not a solution of our left-hand side Hamiltonian.

Once the partial wave solutions of Eq. (14) are obtained, they are summed according to Eq. (13) to build Ψ_{sc} and then used to evaluate the fully differential cross section

$$
\frac{d^8\sigma(\alpha, \beta, \gamma)}{dE_1 d\Omega_1 d\Omega_2 d\alpha d\beta d\gamma}
$$
$$
= \frac{4\pi^2}{\omega c}k_1 k_2\left|\left\langle\Phi^-(\mathbf{r}_1, \mathbf{k}_1)\Phi^-(\mathbf{r}_2, \mathbf{k}_2)\left|\frac{1}{r_{12}}\right|\Psi_{sc}(\mathbf{r}_1, \mathbf{r}_2)\right\rangle\right|^2,
$$
$$(15)$$

where $\Phi^-(\mathbf{r}_i, \mathbf{k}_i)$ are asymptotic states for the ejected electrons scattered by the averaged dication potentials $\mathcal{U}_i(r_i)$, with spherical incoming wave conditions and asymptotic momenta $\mathbf{k}_i$. Because of the simple dependence of Ψ_{sc} on the Wigner matrix, the angular average of the cross section can be performed analytically, so that

$$
\frac{d^5\sigma}{dE_1 d\Omega_1 d\Omega_2}
$$
$$
= \frac{4\pi^2}{\omega c}k_1 k_2 \sum_{L_0}\frac{1}{2L_0 + 1}\sum_{M_0=-L_0}^{L_0}\sum_{L=\mathrm{Max}[0, L_0-1]}^{L_0+1}
$$
$$
\times\left|\left\langle\Phi^-(\mathbf{r}_1, \mathbf{k}_1)\Phi^-(\mathbf{r}_2, \mathbf{k}_2)\left|\frac{1}{r_{12}}\right|\psi_{sc}^{L, M_0}(\mathbf{r}_1, \mathbf{r}_2)\right\rangle\right|^2. \quad (16)
$$

Strictly speaking, this is a fivefold differential cross section, but it is commonly referred to as TDCS.

D. Numerical implementation

The spherical symmetry of the potential makes the calculation of each partial wave very similar to that of helium PDI investigated in Ref. [12]. The main differences are in the structure of the initial states and the central potential for the continuum electrons. For each initial state we have evaluated the weights of each partial-wave term, and cut the series when the cumulative sum reached a value greater than 0.99 (see Table I). Each partial wave of the initial state corresponding to quantum numbers L_0 and M_0 populates a continuum state with quantum numbers $L = L_0$ and $L_0 \pm 1$ for $L_0 > 0$ and $L = 1$ for $L_0 = 0$, while $M = M_0$. This defines a set of equations for the partial-wave terms ψ_{sc}^{L, M_0}, and we could have more than one contribution to each continuum partial wave. Solutions of each three-body equation (14) were obtained through the GSF method as described in Ref. [12]. We found a satisfactory convergence of the TDCS by using a domain of 50 a.u. for each radial coordinate and by expanding each two-dimensional radial function with 50 GSF per radial coordinate. The angular basis for the continuum includes all the possible combinations up to a given maximum value L_{max} of the single electron angular quantum numbers l_1 and l_2; convergence was found with $L_{\mathrm{max}} = 4$. We ended up with linear systems whose size depends on the different angular quantum numbers and spin symmetry, with matrices of the order of a few Gb, which are solved with the preconditioned conjugate gradient squared method, as detailed in Ref. [12]. A few hours are needed to solve the whole set of partial waves corresponding to a given initial state. This computational time could be reduced by considering separately the contributions of the different parities of the initial and final wave functions. Roughly speaking, this procedure would double the number of linear systems while reducing their sizes by a factor two, and thus reducing the computer memory requirements.

E. Comments on the approximations

This model entails several approximations that deserve some comments.

An approximation consists of the description of the target initial state by separable orbitals without correlation. This

choice is guided by the ensuing facility to construct initial two-electron wave functions; this would not be possible starting from a fully correlated 10-electron initial wave function. Moreover, this approximation permits an easy construction of the direct dication potential (the exchange term has been dismissed); a construction from a fully correlated wave function would imply serious complications because one should separate from it the removed electrons before considering the remaining electronic densities.

The angular average of the central potential is another approximation which we believe to be of the same order (if not stronger) than the use of simplified initial states. Through this average, conservation of the total angular-momentum quantum numbers can be applied, making the problem more accessible from the numerical point of view. Without the average, instead of dealing with several linear systems for each of the populated partial waves, we would have a unique huge linear system demanding considerably larger computational resources. So, while feasible, the numerical implementation would simply be much more costly. Besides, as discussed in the results section, the present partial-wave decomposition allows us to make some interesting comparisons with the atomic PDI cases.

With respect to the choice of separable orbitals for the water molecule, for practical and reproducibility reasons we used the one-center tabulated Moccia orbitals which provide fairly well the main geometrical aspects. More accurate, e.g., Hartree Fock, solutions obtained with quantum chemistry packages could be easily envisaged.

All these approximations related to the initial state have certainly some influence on the final calculated cross sections. However, we believe that, at 20 eV above threshold, the final-state correlation of the two electrons in the continuum by far dominates the process and governs the TDCS shapes, as thoroughly observed for the helium case [2]. Within the present theoretical model which is clearly perfectible, the two-electron continuum is treated by an accurate numerical GSF approach.

IV. RESULTS AND DISCUSSION

The electronic configuration of the ground state of the H_2O molecule is described by five doubly occupied molecular orbitals $(1a_1)^2(2a_1)^2(1b_2)^2(3a_1)^2(1b_1)^2 X^1A_1$ [23]. Thus the ground state belongs to the C_{2v} point group and the electronic states are described by using the irreducible representations A_1, A_2, B_1, and B_2. From the four valence orbitals sixteen different double-hole final states can be obtained [24,25]. The nomenclature of orbitals with two electrons removed from the same orbital is given as $(2a1)^{-2}$, $(3a1)^{-2}$, $(1b1)^{-2}$, and $(1b2)^{-2}$, or from two different orbitals $(1b1)^{-1}(3a1)^{-1}$, $(1b1)^{-1}(1b2)^{-1}$, $(1b1)^{-1}(2a1)^{-1}$, $(3a1)^{-1}(1b2)^{-1}$, etc. Experimental information on the dication states of water has been provided by photoion-photoion coincidence experiments [26,27], double charge-transfer measurements [24,28], and Auger spectroscopy [29].

The two previous PDI [6,7] measurements mainly focused on the indirect process at threshold, thus no direct spectroscopic information was provided. As shown in Ref. [10], due to the overall experimental energy resolu-
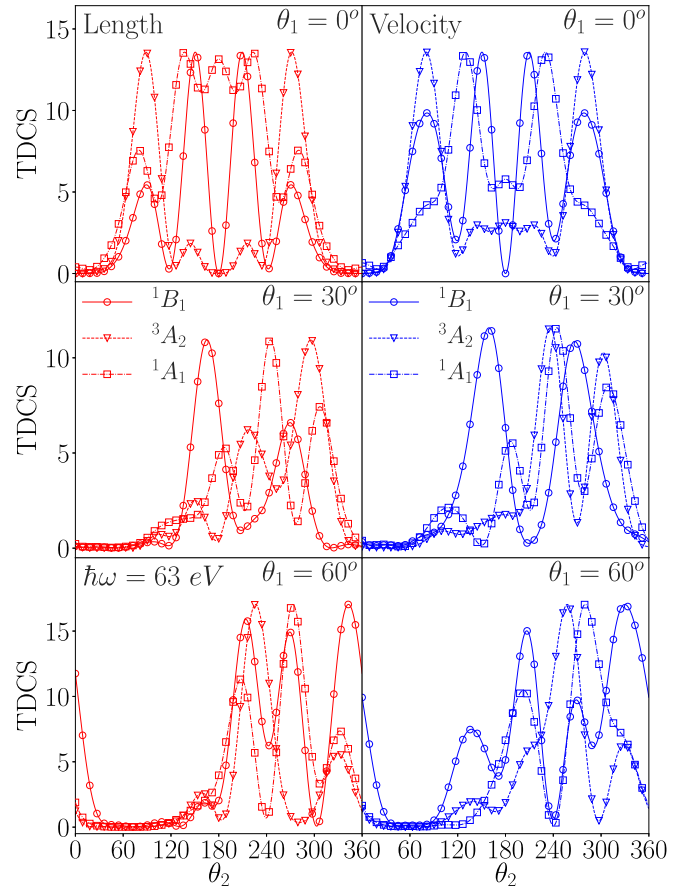

FIG. 2. Theoretical TDCS of water for two electrons ejected with equal energy ($E_1 = E_2 = 10$ eV) and for three fixed θ_1 angles, calculated in both length (left) and velocity (right) gauges for those initial states which contribute to the PDI at 63 eV photon energy. The incident radiation is linearly polarized along the 0° direction.

tion, more than one dication state is involved at both photon energies used in the present experiments. According to the spectroscopy of the water dication states reported in Refs. [24,25], the $(3a_1)^{-1}(1b_1)^{-1}$ $^1B_1$, $(1b_2)^{-1}(1b_1)^{-1}$ $^3A_2$, and $(3a_1)^{-2}$ $^1A_1$ states contribute to the TDCS measured at 63 eV, while the $(1b_2)^{-1}(1b_1)^{-1}$ $^3A_2$, $(3a_1)^{-2}$ $^1A_1$, $(3a_1)^{-1}(1b_2)^{-1}$ $^3B_2$, and $(3a_1)^{-1}(1b_2)^{-1}$ $^1B_2$ ones contribute to the TDCS measured at 65 eV. The binding energies of these two-electron states are reported in Table II.

The calculations have been performed for each one of these initial states in both the length and velocity gauges, for an incident radiation linearly polarized along the 0° direction. The results are shown on an absolute scale in Fig. 2 for 63 eV and in Fig. 3 for 65 eV. Because the contribution of each molecular orbital was not resolved in the experiments, the theoretical results were then used in a global fit of the experimental data at the three angles at each of the two incident energies. The relative contributions of the different states were the free parameters in the weighted linear regression, with the weights corresponding to the inverse of the square of the experimental error. The experimental TDCS at 63 and 65 eV photon energy, together with the theoretical predictions considering

TABLE II. Binding energies for the two-electron states involved in the PDI of water at 63 and 65 eV photon energies.

Photon energy (eV)	H_2O^{2+} states Configuration & symmetry [27,30]		Binding energies (eV) [27]
63	$(3a_1)^{-1}(1b_1)^{-1}$	$^1B_1$	41.94
63 and 65	$(1b_2)^{-1}(1b_1)^{-1}$	$^3A_2$	43.53
63 and 65	$(3a_1)^{-2}$	$^1A_1$	45.35
65	$(3a_1)^{-1}(1b_2)^{-1}$	$^3B_2$	45.48
65	$(3a_1)^{-1}(1b_2)^{-1}$	$^1B_2$	47.76

contributions from different initial states, are shown in Figs. 4 and 5, respectively.

For the data at 63 eV incident energy, the best fit is achieved in both gauges by using the $(1b_2)^{-1}(1b_1)^{-1}$ $^3A_2$ and $(3a_1)^{-2}$ $^1A_1$ states, the first one having a dominant role as indicated by the histogram in Fig. 4. In the case of the data at 65 eV incident energy also the $(3a_1)^{-1}(1b_2)^{-1}$ $^1B_2$ and $^3B_2$ states contribute, with the $^3A_2$ and $^3B_2$ having a dominant role (see histogram in Fig. 5). The important variation in relative contributions with just 2 eV photon energy change, although surprising, can be attributed to the following reasons: First, as indicated by Table II, at 65 eV several more dication states are theoretically accessible and the experiment is effectively observing this through a substantial redistribution of the weights. Second, the vibrational distribution of each state implies a natural overlap; as a consequence, taking into account the

experimental energy resolution, the signal measurement is automatically probing the contribution from a combination of several states at the same time.

The shape of the PDI angular distribution is determined by the combination of the Coulomb repulsion of the two electrons in the continuum and the symmetry of the wave function of the electron pair, defined by the dipole selection rules and the initial-state wave function. In the atomic case, no intensity is generally observed in the half plane where the fixed direction photoelectron is detected, simply because of Coulomb repulsion between the two photoelectrons. In our measurements in water, the angular cross sections (Figs. 4 and 5) are characterized, both experimentally and theoretically, by a multilobe structure with some intensity also in this plane. The TDCS measured at $\theta_1 = 0°$ displays, as expected, a symmetry about the direction of the polarization axis of the incident radiation, which coincides with the direction of
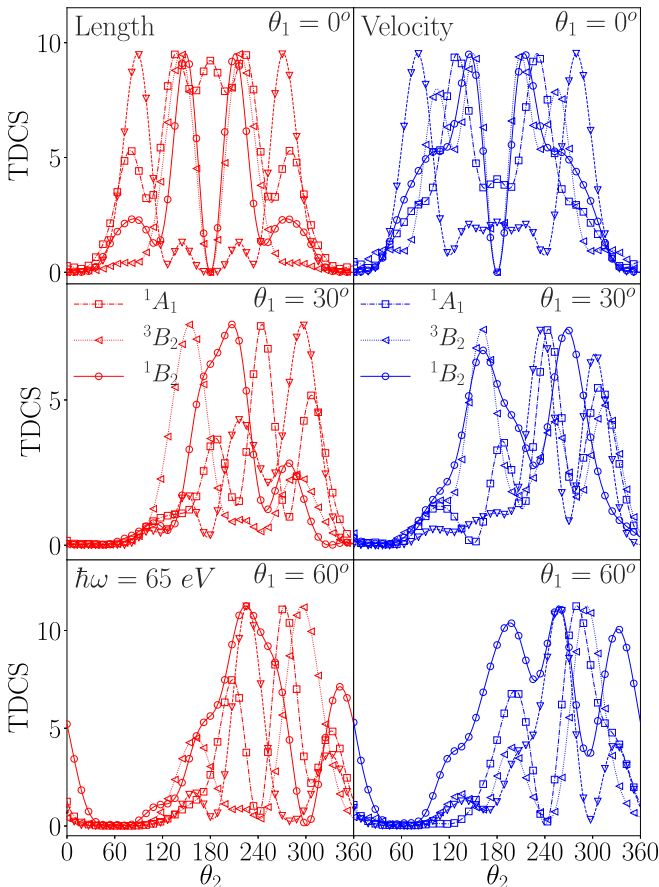

FIG. 3. Same as in Fig. 2 but for those initial states which contribute to the PDI at 65 eV photon energy.
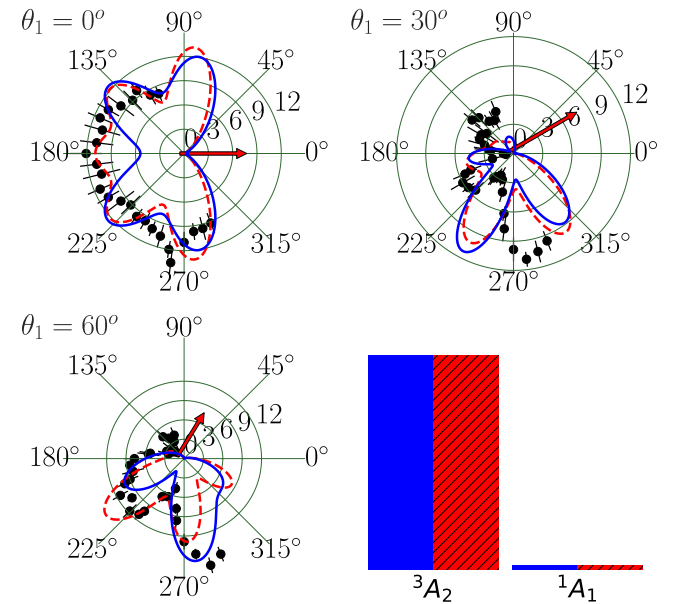

FIG. 4. The TDCS of water measured at 63 eV photon energy in the condition of equal energy sharing ($E_1 = E_2 = 10$ eV) for three fixed directions θ_1 (red arrows) of one photoelectron compared with the theoretical predictions in the length (dashed red curves) and velocity (solid blue curves) gauges. The incident radiation is fully linearly polarized along the 0°-180° direction. In the bottom-right histogram the contributions of the different dication states are reported (blue bars for velocity gauge, red dashed bars for length gauge).
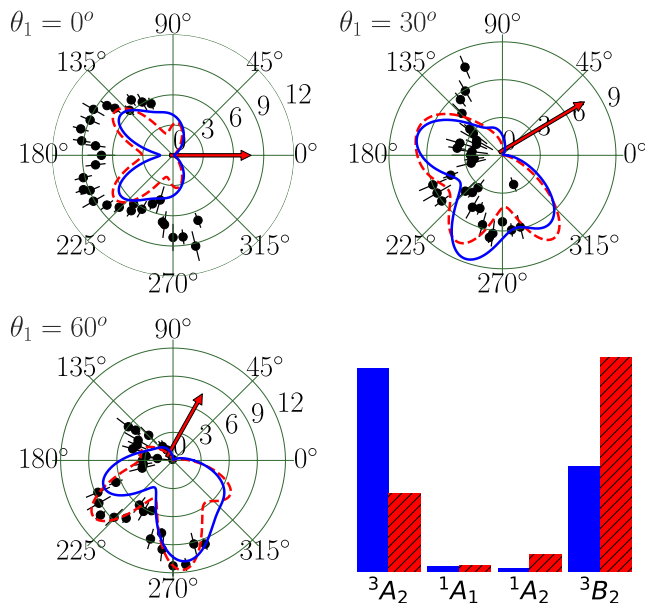
FIG. 5. Same as in Fig. 4 but at 65 eV photon energy.

FIG. 6. The TDCS of water measured at 63 eV photon energy for fixed direction $\theta_1 = 0°$ (red arrow) of one photoelectron compared with the theoretical predictions in the length (dashed red curve) and velocity (solid blue curve) gauges. The incident radiation is fully linearly polarized along the $0°-180°$ direction. In the histogram the contributions of the different dication states are reported (blue bars for velocity gauge, red dashed bars for length gauge).

detection of one photoelectron. The signal is concentrated in the half plane opposite to the direction of the photoelectron detected by the fixed analyzer. The most remarkable feature in the measured TDCS is the large intensity in the back-to-back direction ($\theta_1 - \theta_2 = \theta_{12} = 180°$): it corresponds to a maximum for $\theta_1 = 0°$ and $30°$ in the $\hbar\omega = 63$ eV case and for $\theta_1 = 30°$ in the $\hbar\omega = 65$ eV case, while a shallow minimum is observed in the other configurations.

According to the present theoretical calculations, this back-to-back emission arises from the $(3a_1)^{-2}$ $^1A_1$ and the $(1b_2)^{-1}(1b_1)^{-1}$ $^3A_2$ initial states. In atoms [31], TDCS maxima and minima are associated with the nodal properties of the electron pair wave function, and are therefore related to its angular momentum, spin, and parity. For example, triplet states including partial waves with $l_1 = l_2$ quantum numbers must vanish in the $r_1 = r_2 \to \infty$ asymptotic region, leading to a zero back-to-back contribution; on the other hand, due to the population of the $^1S^e$ and $^1D^e$ continuum partial waves, the double ionization of argon to the $3s3p^5$ $^1P^o$ Ar^{2+} state [32], has a maximum in that geometrical configuration. As shown in Table I, in the water molecule, many partial waves contribute to the initial states. Each of them ends up populating a continuum partial wave with different parity. Similarly to argon, for the $(3a_1)^{-2}$ $^1A_1$ state we have also found that the $^1S^e$ and $^1D^e$ partial waves are those which contribute to the back-to-back emission for singlet symmetry at equal energy. In the case of the $(1b_2)^{-1}(1b_1)^{-1}$ $^3A_2$ initial state, on the other hand, the $^3P^o$ and to a lesser extent the $^3F^o$ partial wave are those contributing to the back-to-back emission. The other initial states have components that are practically negligible in the mentioned geometry. One should keep in mind, however, that the theoretical relative population of the different partial waves may change with a better description of the interactions, for example by taking a more elaborate molecular dication potential for the outgoing electrons, or by adding electron-electron correlation in the initial states.
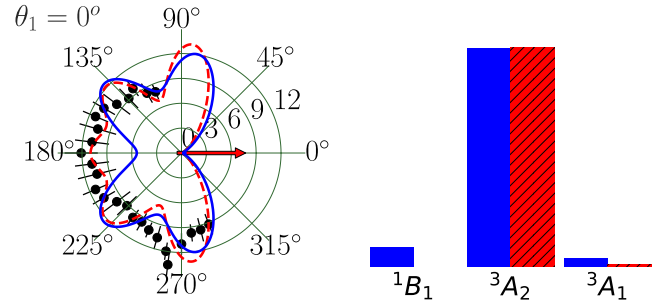
The multilobe structure observed for $\theta_1 = 0°$ evolves when moving to the two larger θ_1 values. At $\theta_1 = 30°$ three lobes can be envisioned with comparable intensity at 65 eV, while at 63 eV the emission is enhanced at about $\theta_{12} = 100°$. Also, in this case, the experiments display a nonvanishing intensity in the back-to-back direction. For both measured energies and $\theta_1 = 60°$, the lobe at about $\theta_{12} = 135°-150°$ appears to be the dominant feature. In contrast with the other two θ_1 angles, in this case a clear minimum in the TDCS is observed in the back-to-back direction.

We can state that a global agreement between the shape of the theoretical predictions and the experimental data exists, even though the overall *simultaneous* fit to all three TDCS measured at the same energy yields different relative intensities between predicted and measured features. For example, a large difference in magnitude between theoretical and experimental results appears for $\theta_1 = 0$, although the angular distribution seems to be well described by the length gauge results. To better identify the structures of the angular distributions which are also present in the theoretical model, for this geometry we have fit the data independently from the other two θ_1 cases. Figure 6 shows, for 63 eV, the obtained fitted TDCS and the relative intensities of the states involved. Similarly to what we found with the complete fit presented in Fig. 4, we have a large contribution from the $(1b_2)^{-1}(1b_1)^{-1}$ $^3A_2$ state and to a lesser extent from the $(3a_1)^{-2}$ $^1A_1$ one. A small contribution from the $(3a_1)^{-1}(1b_1)^{-1}$ $^1B_1$ state also appears now but only for the velocity gauge. The experimental shallow maximum in the back-to-back direction is reproduced by the length gauge calculation only, while the other two peaks located at symmetrical position from $\theta_2 = 180°$ are predicted in both gauges, with a $20°$ difference with respect to the observed peak position. The experimental lobe at $\theta_2 \sim 270°$ is approximately reproduced in both gauges, and the relative intensities of the peaks also agree with the measurement.

The general shape and number of peaks predicted by the theoretical calculations can be recognized in the experiment. While this is remarkable, considered the approximations made in the model, some features are wrong or not observed. One noticeable difference is the position of the principal lobes for $\theta_1 = 30°$, at both energies, which seems to be wrongly

predicted by the contributions of both the $(3a_1)^{-2}$ $^1A_1$ and $(3a_1)^{-1}(1b_2)^{-1}$ $^3B_2$ states to the theoretical TDCS. Another difference is that theory predicts at both $\theta_1 = 30°$ and $60°$ a minimum at $\theta_{12} = 180°$, while in the experiments we observe a minimum only at $\theta_1 = 60°$. A large difference between theory and experiment is also observed for the width of the TDCS at $\theta_1 = 0°$ and $\hbar\omega = 63$ eV in the velocity gauge, while for the length gauge the relative intensity predicted by the global fit appears to be definitely too low.

The general structure of the theoretical lobes can be analyzed through inspection of the two-electron continuum partial waves. At both energies, the TDCS lobe for $\theta_1 = 60°$ at $\theta_{12} \simeq 225°$ comes mainly from the $^1P^o$ and $^1S^e$ terms excited from the S, P, and D components of the $(3a_1)^{-2}$ $^1A_1$ state, the $^3F^e$ from the D initial component of $(1b_2)^{-1}(1b_1)^{-1}$ $^3A_2$, and $^1D^e$, $^3F^o$, and $^3G^e$ coming from P, D, and F components of the $(3a_1)^{-1}(1b_2)^{-1}$ $^1A_2$ state. The other important lobe is located at $\theta_{12} \simeq 270°$. The partial waves contributing to it were found to be the ^3F e and o components coming from D partial waves of the $(1b_2)^{-1}(1b_1)^{-1}$ $^3A_2$ initial state, and the $^1P^o$, $^1D^o$, and $^1F^e$ ones arising from P and D initial components of the $(3a_1)^{-1}(1b_2)^{-1}$ $^1A_2$.

One final comment: since the initial and final states are not calculated with the same potential, one should not expect gauge invariance. Also, the independent model description of the initial state is not at all equivalent to the fully correlated two-electron continuum. In spite of this, and probably due to the orientation average, a rather good global agreement between the two gauges is observed. The exception, as already mentioned, is the case of the TDCS at $\theta_1 = 0°$ and $\hbar\omega = 63$ eV.

V. CONCLUSIONS

The photodouble ionization of the water molecule has been studied at 20 eV excess and equal energy sharing, in a combined experimental and theoretical work. The TDCS at 63 and 65 eV photon energies have been measured by the coincidence detection of the outgoing electrons and calculated by using products of single-electron Moccia orbitals referred to a single center for the initial states, and the generalized Sturmian function approach for the evolution of the two-electron wave function in the continuum. The use of the Wigner matrix for the rotation of the spherical harmonics allows for an analytical average of the cross sections over the (experimentally undetected) molecular orientation.

Considering the complex structure of the water molecule, a reasonably good qualitative agreement between theory and experiment has been found. The possibility to refer the two-electron dynamics to the oxygen position and the decomposition of the initial states in eigenfunctions of the total angular momentum enabled us to analyze the different contributions to the TDCS shapes.

Our theoretical model can be improved along several lines such as a better description of the initial state and the consideration of the molecular structure of the dication potential. These perspectives entail a completely different structure of the final system of linear equations to be solved and a different orientation average procedure for the TDCS; such important changes are the subject of future investigations.

As presented here, our theoretical method is not limited to a triatomic molecule like water, but can be extended also to other polyatomic molecules. This will pave the way to the investigation of PDI by photoelectron-photoelectron coincidence in systems, like aromatic compounds, where collective excitations or more intriguing mechanisms affect PDI [33].

[1] L. Avaldi and A. Huetz, J. Phys. B: At., Mol. Opt. Phys. **38**, S861 (2005).

[2] J. S. Briggs and V. Schmidt, J. Phys. B: At., Mol. Opt. Phys. **33**, R1 (2000).

[3] P. Bolognesi, R. Camilloni, M. Coreno, G. Turri, J. Berakdar, A. S. Kheifets, and L. Avaldi, J. Phys. B: At., Mol. Opt. Phys. **34**, 3193 (2001).

[4] T. Weber *et al.*, Nature (London) **431**, 437 (2004).

[5] T. J. Reddish, J. Colgan, P. Bolognesi, L. Avaldi, M. Gisselbrecht, M. Lavollee, M. S. Pindzola, and A. Huetz, Phys. Rev. Lett. **100**, 193001 (2008).

[6] S. Y. Truong, A. J. Yencha, A. M. Juarez, S. J. Cavanagh, P. Bolognesi, and G. C. King, Chem. Phys. Lett. **474**, 41 (2009).

[7] J. H. D. Eland, Chem. Phys. **323**, 391 (2006).

[8] D. Reedy, J. B. Williams, B. Gaire, A. Gatton, M. Weller, A. Menssen, T. Bauer, K. Henrichs, P. Burzynski, B. Berry *et al.*, Phys. Rev. A **98**, 053430 (2018).

[9] Z. L. Streeter, F. L. Yip, R. R. Lucchese, B. Gervais, T. N. Rescigno, and C. W. McCurdy, Phys. Rev. A **98**, 053429 (2018).

[10] G. Turri, P. Bolognesi, H. Sugimoto, J. Mathis, and L. Avaldi, J. Phys. B: At., Mol. Opt. Phys. **52**, 07LT01 (2019).

[11] P. Bolognesi, B. Joulakian, A. A. Bulychev, O. Chuluunbaatar, and L. Avaldi, Phys. Rev. A **89**, 053405 (2014).

[12] J. M. Randazzo, D. Mitnik, G. Gasaneo, L. U. Ancarani, and F. D. Colavecchia, Eur. Phys. J. D **69**, 189 (2015).

[13] F. L. Yip, T. N. Rescigno, and C. W. McCurdy, Phys. Rev. A **94**, 063414 (2016).

[14] A. S. Kheifets and I. Bray, Phys. Rev. A **72**, 022703 (2005).

[15] W. Vanroose, F. Martin, T. N. Rescigno, and C. W. McCurdy, Phys. Rev. A **70**, 050703(R) (2004).

[16] R. Moccia, J. Chem. Phys. **40**, 2164 (1964).

[17] P. Bolognesi, M. Coreno, G. Alberti, R. Richter, R. Sankari, and L. Avaldi, J. Electron Spectrosc. Relat. Phenom. **141**, 105 (2004).

[18] C. M. Granados-Castro and L. U. Ancarani, Eur. Phys. J. D **71**, 65 (2017).

[19] L. Fernández-Menchero and S. Otranto, Phys. Rev. A **82**, 022712 (2010).

[20] L. Fernández-Menchero and S. Otranto, J. Phys. B: At., Mol. Opt. Phys. **47**, 035205 (2014).

[21] G. W. F. Drake, *Springer Handbook of Atomic, Molecular, and Optical Physics* (Springer, New York, 2006).

[22] A. R. Edmonds, *Angular Momentum in Quantum Mechanics* (Princeton University Press, Princeton, 1957).

[23] O. Dutuit, A. Tabche-Fouhaile, I. Nenner, H. Frohlich, and P. M. Guyon, J. Chem. Phys. **83**, 584 (1985).

[24] V. Carravetta and H. Ågren, Phys. Rev. A **35**, 1022 (1987).

[25] L. Inhester, C. F. Burmeister, G. Groenhof, and H. Grubmüller, J. Chem. Phys. **136**, 144304 (2012).

[26] P. J. Richardson, J. H. D. Eland, P. G. Fournier, and D. L. Cooper, J. Chem. Phys. **84**, 3189 (1986).

[27] D. Winkoun, G. Dujardin, L. Hellner, and M. J. Besnard, J. Phys. B: At., Mol. Opt. Phys. **21**, 1385 (1988).

[28] J. C. Severs, F. M. Harris, S. R. Andrews, and D. E. Parry, Chem. Phys. **175**, 467 (1993).

[29] H. Siegbahn, L. Asplund, and P. Kelfve, Chem. Phys. Lett. **35**, 330 (1975).

[30] B. Gervais, E. Giglio, L. Adoui, A. Cassimi, D. Duflot, and M. E. Galassi, J. Chem. Phys. **131**, 024302 (2009).

[31] C. H. Greene and A. R. P. Rau, Phys. Rev. Lett. **48**, 533 (1982).

[32] J. Mazeau, P. Lablanquie, P. Selles, L. Malegat, and A. Huetz, J. Phys. B: At., Mol. Opt. Phys. **30**, L293 (1997).

[33] R. Wehlitz, P. N. Juranić, K. Collins, B. Reilly, E. Makoutz, T. Hartman, N. Appathurai, and S. B. Whitfield, Phys. Rev. Lett. **109**, 193001 (2012).